

M³RS: Multi-robot, Multi-objective, and Multi-mode Routing and Scheduling

Ishaan Mehta[†], Junseo Kim[†], Sharareh Taghipour[†] and Sajad Saeedi[†]

Abstract—The quality of task execution can significantly impact a multi-robot mission. While higher quality is desirable, it may not always be feasible due to mission constraints. Existing multi-robot task allocation literature generally overlooks quality of service as a decision variable. Addressing this gap, we introduce the multi-robot, multi-objective, and multi-mode routing and scheduling (M³RS) problem, designed for time-bound, multi-robot, multi-objective missions. In M³RS, each task offers multiple execution modes, each with different resource requirements, execution time, and quality. M³RS optimizes task sequences and execution modes for each agent. The need for M³RS comes from multi-robot applications in which a trade-off between multiple criteria can be achieved by varying the task level quality of service through task execution modes. Such ability is particularly useful for service robot applications. We use M³RS for the application of multi-robot disinfection in healthcare environments and other public locations. The objectives considered for disinfection application are disinfection quality and number of tasks completed. A mixed-integer linear programming (MIP) model is proposed for M³RS. Further, a clustering-based column generation (CCG) algorithm is proposed to handle larger problem instances. Through synthetic, simulated, and hardware case studies, we demonstrate the advantages of M³RS, showing it provides flexibility and strong performance across multiple metrics. Our CCG algorithm generates solutions 2.5× faster than a baseline MIP optimizer, maintaining competitive performance. The videos for the experiments are available on the project website¹.

Index Terms—multi-robot system, autonomous systems, task allocation, scheduling, service robots, disinfection robots.

I. INTRODUCTION AND RELATED WORKS

Maintaining hygiene in healthcare environments is crucial to prevent catastrophic issues like hospital-acquired infections. Disinfection robots are useful technologies that provide an additional layer of protection by automating the disinfection of target surfaces. A team of these robots can improve both spatial and temporal efficiency in maintaining hygiene standards in hospitals [1]. To coordinate a fleet of robots for a disinfection mission, two key decisions must be made: i) which task will be assigned to which robot, and ii) what level of disinfection quality should be applied to each task. While higher disinfection quality is desirable, it also requires more time and resources, which may not always be feasible. The assignment of tasks to robots has been studied in the literature [2], but there is a lack of research addressing the decision regarding the quality of service of a task. In disinfection applications, considering the quality of tasks is important as it impacts overall hygiene standards. Additionally, some surfaces, such as those in patient rooms and ICUs, require stringent quality standards. In this work, we tackle the problem of deciding which tasks to implement and at what mode/quality.

For a team of robots, Multi-robot Task Allocation (MRTA) algorithms [3, 2] allocate tasks to various robots working on a

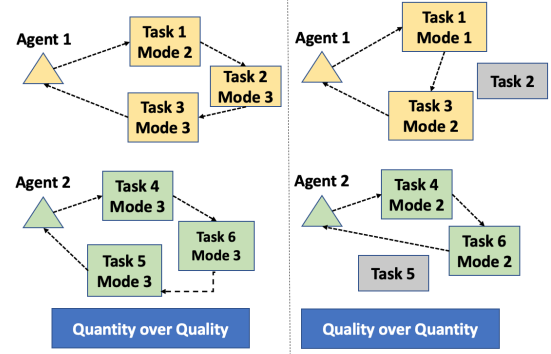


Figure 1. M³RS is suitable for routing and scheduling in time-bound scenarios where multiple criteria of interest depend on the mode in which the agents execute the tasks. This visualization depicts two cases. Here, mode 1 stands for the highest quality and long task execution times, whereas mode 3 is for the lowest quality and fastest task execution times. The left side of the image shows a case where agents choose to maximize the number of tasks completed by performing tasks in lower-quality modes. On the right, agents prioritize quality over quantity. As a result, tasks 2 and 5 are missed. An example of such a scenario is a multi-robot system performing services such as disinfection and cleaning.

common mission while optimizing a joint mission objective. A key metric to evaluate these allocations is the quality of service (QoS) for the mission. The definition of QoS depends on the mission requirements and target application, such as the quality of communication between the robot and the base station [4, 5], the tardiness of addressing tasks [6], the average waiting time for a customer [7], or productivity and fatigue [8]. Often, there is a trade-off between QoS and other mission objectives, which could be conflicting. In such cases, multiple solutions exist that prioritize these objectives [4, 5, 8].

MRTA problems are \mathcal{NP} -hard, making larger instances challenging to solve. With extra variables, concerning the quality of the service, the problem becomes more complex. Techniques such as heuristics and metaheuristics are faster but often sacrifice optimality [9]. Learning-based methods require expensive training and massive datasets, and may still struggle to generalize [10]. Column generation is a decomposition approach that refines the solution iteratively by solving smaller sub-problems. This allows faster convergence to higher-quality solutions as it directly exploits the problem’s structure and efficiently handles large-scale instances. We propose a clustering-based column generation algorithm, where clustering further helps in reducing the search space to find good quality solutions.

To the best of our knowledge, this is the first work to address task-level service quality using multiple execution modes for quality-dependent multi-robot missions. We introduce a multi-robot, multi-objective, and multi-mode routing and scheduling (M³RS) problem. The contributions of this work are:

- 1) We present M³RS, a novel problem to alter task-level QoS to achieve trade-offs in different mission objectives. The proposed problem is well-suited for applications where tasks are spread across a physical space, each

[†]Toronto Metropolitan University
Email: {ishaan.mehta, junseo.kim, sharareh, s.saeedi}@torontomu.ca
¹<https://sites.google.com/view/g-robot/m3rs/>

task has service requirements and resource requirements, and the overall mission has multiple criteria of interest. Each robot can address the task in multiple execution modes, where each mode corresponds to different task quality, resource consumption, and service times. A visual depiction of the application of M³RS is given in Fig. 1.

- 2) We present the usage of M³RS for a multi-robot disinfection application. A thorough study of different mission scenarios is conducted on a synthetic dataset. Further, we test M³RS in simulated and hardware case studies.
- 3) We use a mixed-integer linear programming formulation for the proposed problem. To handle the large decision space, we propose clustering-based column generation (CCG) for solving M³RS. CCG generates solutions 2.5× faster than the baseline while maintaining competitive performance.

This paper is organized as follows: The general formulation and optimization of M³RS is given in Section III. The results of the synthetic, simulated, and real-world experiments are presented in Section IV. Finally, Section V includes future works and conclusions.

II. LITERATURE REVIEW: QoS IN TASK ASSIGNMENT

QoS has also received attention in routing and production scheduling literature. Exposito et al. [11] considered the timeliness of vehicles as a QoS indicator for vehicle routing. Similarly, QoS has been studied for home healthcare applications, where it involves routing nurses to different patients for healthcare-related services, depending on the patient receiving care from a nurse with the desired experience [12, 13]. In supply chain and production planning, QoS has been considered as the existence of minimum stock [14]. Most of these existing works modify the task allocation to achieve different trade-offs between QoS and other objectives. However, there are no works that focus on the deliberate degradation or improvement of QoS offered to an individual task by a robot as a means to achieve an overall trade-off for various mission objectives.

Task execution modes are different operational settings for servicing tasks. These modes depend on various constraints in the environment or aim to achieve desired performance on key metrics like quality and resource consumption. Lahijanian et al. [15] explored using an energy-saving mode where resource-intensive autonomy features are disabled to conserve energy in resource-constrained environments. The usage of task execution modes in MRTA has been limited. Task execution modes were used to decide if humans and robots should collaborate to maximize time efficiency [16, 17]. In project scheduling, task execution modes are used to minimize project makespan while adhering to resource constraints [18, 19, 20]. In vehicle routing, mode selection involves choosing delivery locations with specific constraints, impacting customer delivery [21]. The hybrid electric vehicle routing problem in [22] used mode selection for switching driving modes, affecting emissions and transportation costs. Using task execution modes to select QoS provided to the task is still unexplored. This decision affects

the quality of individual tasks and the overall mission. For example, in a disinfection mission, cleaning a surface with the highest available dosage ensures the highest quality level. However, higher dosages require longer service times, which could potentially result in skipping other tasks.

III. MULTI-ROBOT MULTI-OBJECTIVE MULTI-MODE ROUTING AND SCHEDULING

In this section, first, the general optimization model for M³RS problem is presented. Then we present a column generation (CG) scheme to solve the optimization model with faster computation times. Our novel contribution is the use of clustering heuristics, which helps solve the problem more quickly and find solutions with better objective values. Finally, the formulation is applied to the multi-robot disinfection application.

Table I
NOTATION FOR M³RS.

Notation	Description
\mathcal{A}	Set of agents.
\mathcal{T}	Set of tasks.
\mathcal{M}_i	Set of modes for task i , where $\mathcal{M}_i = \{1, 2, \dots, M\}$.
R	Number of objective criteria.
f_r	r^{th} objective criterion.
$p_{i,m}$	The quality indicator of doing task i in mode m .
p^{max}	The highest possible quality of disinfection
$\sigma_{i,m}$	Time to complete task i in mode m .
$q_{i \rightarrow j}$	Energy consumed for travelling from task i to task j .
q_{idle}^k	Energy consumption during idling by agent k .
$q_{i,m}$	Energy consumption of task i in mode m .
q_{travel}	Avg. current consumption in traveling at a constant speed.
q_{tc}	Avg. current consumption while completing tasks.
q_{idling}	Avg. current consumption while idling.
$[a_i, b_i]$	Start and end time for task i .
Q	Total capacity of an agent.
T_H	Time available to complete all tasks.
$t_{i,j}$	Travel time from task i to task j .
λ_r	The scalar preference for r^{th} objective function.
s_i^k	A decision variable for arrival time of agent k to task i .
$x_{i \rightarrow j}^k$	A binary decision variable for if agent k goes from task i to task j .
$y_{i,m}^k$	A binary decision variable for task i done in mode m by agent k .
η	The load factor hat is used to simulate different disinfection missions.

A. Optimization Model

A solution for the M³RS problem determines routes, schedules, and task execution modes for a set of agents \mathcal{A} , and a set of tasks \mathcal{T} distributed across physical space. Refer to Table I for notation. All the agents are identical, and only one agent can service each task. We use i and j to denote different tasks in \mathcal{T} and k to denote k^{th} agent in the rest of the notation. The time window for a task i specifies a starting time, a_i , and finishing time, b_i , within which the task must be serviced. The entire multi-robot operation must be done in a fixed mission time of T_H hours. Further, each task i has an associated mode set $\mathcal{M}_i = \{1, 2, \dots, M\}$, representing available task service modes. Each task can have distinct modes of service available, so each task has a distinct mode set. An agent services the task in one of the modes available in the associated mode set. The selected mode $m \in \mathcal{M}_i$ for task i has

a corresponding service time ($\sigma_{i,m}$) and energy requirement ($q_{i,m}$) from the agent. Performing a task in a mode with higher service time and resource consumption would lead to lower availability of agents for other tasks. The overall scheduling and allocation mission is optimized for multiple objectives.

The energy capacity for each agent is given by Q Ah (Ampere-hours). The energy consumption for each agent is divided into performing tasks, traveling, and idling [23]. A fixed-rate battery model is used to calculate the energy consumption, where energy consumed is proportional to idling time, task execution time, and traveling time respectively [23]. Different aspects of energy expenditure can be calculated using:

$$\begin{aligned} q_{i \rightarrow j} &= q_{\text{travel}} \cdot t_{i,j}, \quad (\text{i.e. traveling energy}) \\ q_{i,m} &= q_{\text{tc}} \cdot \sigma_{i,m}, \quad (\text{i.e. servicing energy}) \\ q_{\text{idle}}^k &= q_{\text{idle}} \cdot (M_k - W_k). \quad (\text{i.e. idling energy}) \end{aligned} \quad (1)$$

Here, q_{travel} is the current consumption for an agent traveling at a constant speed, q_{tc} is the current consumption while performing a task, and q_{idle} is the current consumption for idling. M_k is the total time spent by agent k on the mission, and W_k is the total time spent by agent k traveling and executing tasks. The net energy consumed by agent k in a mission is given by the LHS of Eq. (9). The relevant notation for the formulation is summarised in Table I.

The formulation for M³RS is expressed as a mixed integer with the following decision variables:

- i) the binary decision variable $x_{i \rightarrow j}^k \in \{0, 1\}$ for assignment and transition of agent k from task i to j ;
- ii) the binary decision variable $y_{i,m}^k \in \{0, 1\}$ for allocation of mode m for task i when executed by agent k ; and
- iii) the real continuous variable $s_i^k \in \mathbb{R}$ denotes arrival time of agent k to task i .

The optimization problem is expressed as:

$$\max_{x_{i \rightarrow j}^k, y_{i,m}^k, s_i^k} \sum_{r=0}^R \sum_{k \in \mathcal{A}} \sum_{i \in \mathcal{T}} \sum_{j \in \mathcal{T}} \sum_{m \in \mathcal{M}_i} \lambda_r \cdot f_r(x_{i \rightarrow j}^k, y_{i,m}^k, s_i^k), \quad (2)$$

subject to the constraints in Eq. (3)-(16).

Eq. (2) is the scalar objective function that maximizes the convex combination of R objective criteria. Here, f_r is r^{th} objective criteria for $r = 1, 2, \dots, R$. The user-specified parameter λ_r represents trade-off preference for r^{th} objective criterion. Each objective criterion can depend on task allocation, selected mode, and arrival times.

The constraints of the optimization are categorized into five sets as follows: 1) task assignment constraint, 2) feasibility constraints, 3) energy consumption constraint, 4) time constraints, and 5) domain and preference constraints. These constraints are described next.

1) *Task Assignment Constraint*: Given by Eq. (3), the task assignment constraint ensures that each task is done at most once:

$$\sum_{k \in \mathcal{A}} \sum_{j \in \mathcal{T}} x_{i \rightarrow j}^k \leq 1 \quad \forall i \in \mathcal{T} \setminus 0. \quad (3)$$

Here, $i = 0$ is excluded ($\mathcal{T} \setminus 0$) as it corresponds to the home depot. This is done to maintain feasibility as all agents must leave the home depot. There might be missions where some tasks must be completed. For such cases, the inequality can be replaced by equality for tasks that must be completed.

2) *Feasibility Constraints*: Given by Eq. (4)-(8), the feasibility constraints ensure the solutions are logical.

$$x_{i \rightarrow i}^k = 0 \quad \forall k \in \mathcal{A} \quad \forall i \in \mathcal{T}, \quad (4)$$

$$\sum_{i \in \mathcal{T}} x_{i \rightarrow 0}^k = 1 \quad \forall k \in \mathcal{A}, \quad (5)$$

$$\sum_{j \in \mathcal{T}} x_{0 \rightarrow j}^k = 1 \quad \forall k \in \mathcal{A}, \quad (6)$$

$$\sum_{i \in \mathcal{T}} x_{i \rightarrow h}^k - \sum_{j \in \mathcal{T}} x_{h \rightarrow j}^k = 0 \quad \forall h \in \mathcal{T}, \quad \forall k \in \mathcal{A}, \quad (7)$$

$$\sum_{j \in \mathcal{T}} x_{i \rightarrow j}^k - \sum_{m \in \mathcal{M}_i} y_{i,m}^k = 0 \quad \forall (k, i) \in \mathcal{A} \cup \mathcal{T} \setminus 0. \quad (8)$$

The constraint in Eq. (4) eliminates infeasible solutions where an agent transitions between the same task. The constraints in Eq. (5)-(6) ensure that all agents leave the home depot and return to the home depot, respectively. The constraint in Eq. (7) ensures that the agent must exit the tasks they visit. The constraint in Eq. (8) enforces that each task i can be performed in only one of the modes in \mathcal{M}_i . Thus, for any task i selected by agent k , only one execution mode is used.

3) *Energy Consumption Constraint*: As described by Eq. (9), the energy consumption constraint enforces that the energy expenditure of an agent in the form of traveling, doing tasks, and idling does not exceed the agent's capacity:

$$q_{\text{idle}}^k + \sum_{i \in \mathcal{T}} \left(\sum_{m \in \mathcal{M}_i} q_{i,m} \cdot y_{i,m}^k + \sum_{j \in \mathcal{T}} q_{i \rightarrow j} \cdot x_{i \rightarrow j}^k \right) \leq Q \quad \forall k \in \mathcal{A}. \quad (9)$$

4) *Time Constraints*: Given by Eq. (10)-(12), the time constraints ensure the timing of the tasks are consistent:

$$s_i^k + \sum_{m \in \mathcal{M}_i} \sigma_{i,m} \cdot y_{i,m}^k + t_{i,j} - s_j^k \leq 0 \quad \forall i \in \mathcal{T} \quad \forall j \in \mathcal{T} \quad \forall k \in \mathcal{A}, \quad (10)$$

$$a_i \leq s_i^k + \sum_{m \in \mathcal{M}_i} \sigma_{i,m} \cdot y_{i,m}^k < b_i \quad \forall i \in \mathcal{T}, \quad \forall k \in \mathcal{A}, \quad (11)$$

$$0 \leq s_0^k < T_H \quad \forall k \in \mathcal{A}. \quad (12)$$

The constraint in Eq. (10) ensures that the arrival time for a subsequent task is always later than the previous task. This constraint also enables sub-tour elimination [24], where sub-tours are infeasible solutions that represent disjoint sequences of completing tasks for the same agent. The constraint in Eq. (11) ensures that the agent arrives and completes the task in the selected mode within the task's prescribed time window. Finally, the constraint in Eq. (12) ensures that all agents return to the depot within the specified time horizon T_H .

5) *Domain and User Preference Constraints*: Given by Eq. (13)-(16), the preference constraints ensure the variable and parameters follow the definitions:

$$x_{i \rightarrow j}^k \in \{0, 1\}, \quad (13)$$

$$y_{i,m}^k \in \{0, 1\}. \quad (14)$$

$$0 < \lambda_r \leq 1, \quad (15)$$

$$\sum_{r=0}^R \lambda_r = 1. \quad (16)$$

The constraints in Eq. (13)-(14) enforce binary values for $x_{i \rightarrow j}^k$ and $y_{i,m}^k$, while Eq. (15)-(16) ensure convexity according to given user preferences.

B. A Solution for M³RS: Clustering-based Column Generation

M³RS extends traditional routing and scheduling problems by adding the decision of mode selection, which impacts task quality. Routing and scheduling problems are known to be \mathcal{NP} -hard [25]. Consequently, larger problem instances with many tasks and agents lead to exponential growth in the solution space and significantly burden computational resources [26]. We use CG [27, 28], to address the computational challenges associated with the large decision variables in the proposed formulation. The strength of CG lies in its ability to break down a complex problem into manageable sub-problems while iteratively refining the solution.

The CG algorithm decomposes the original optimization problem into a master problem and a sub-problem. The master problem identifies optimal columns (or paths/solutions) from a pool of feasible candidate solutions, Ω . Since Ω is very large, typically, a restricted master problem is solved on a subset $\Omega' \subset \Omega$. The sub-problem uses the dual solution from the master problem to find new favorable columns, which are added to Ω' to improve the objective value of the master problem. The master problem and sub-problem are solved iteratively until there are no new columns with positive reduced cost. We refer to our approach as CCG (clustering-based CG) due to the use of clustering-based heuristics for solving the sub-problem. The rest of the section presents the building blocks of our CCG algorithm.

1) *Restricted Master Problem*: This problem aims to identify the best set of solutions from the existing solution pool, resembling a set covering problem. Therefore, to solve the restricted master problem, we adopt a set covering problem formulation [27]. A solution for the set covering problem selects a subset of sets (in our case, task sequence and modes for each agent) from a collection (the solution pool Ω') such that most of the elements (tasks) are covered. This must be done while adhering to constraints, such as each task being assigned to only one agent, and maximizing the given objective. The set covering formulation-based restricted master problem finds optimal solutions from a subset of feasible candidate solutions Ω' . Each candidate in Ω' is a feasible solution that specifies a sequence of addressing different tasks in the associated modes and arrival times. The pool Ω' can be initialized by some trivial solutions and can be updated

iteratively with better solutions obtained by solving the sub-problem. The set covering formulation for our restricted master problem is given by:

$$\max_{\theta^k} \sum_{k \in \Omega'} c_k \cdot \theta^k \quad (17)$$

subject to:

$$\sum_{k \in \Omega'} a_i^k \cdot \theta^k \leq 1 \quad \forall i \in \mathcal{T} / \{0\}, \quad (18)$$

$$\sum_{k \in \Omega'} b_{i,m}^k \cdot \theta^k \leq 1 \quad \forall i \in \mathcal{T} / \{0\}, \forall m \in \mathcal{M}_i \quad (19)$$

$$\sum_{k \in \Omega'} \theta^k \leq |\mathcal{A}|, \quad (20)$$

$$\theta^k \in \{0, 1\} \quad (21)$$

Here, θ^k is a binary solution selection variable, where $\theta^k = 1$ if solution $k \in \Omega'$ is selected, and $\theta^k = 0$ otherwise. The objective function in Eq. (17) selects the candidates from Ω' that maximizes the original objective function Eq. (23). The constraint in Eq. (18) ensures that each task in \mathcal{T} is assigned at most once. Here, a_i^k is 1 if i^{th} task is covered in k^{th} solution. The constraint in Eq. (19) ensures that mode m for task i is used at most once with $b_{i,m}^k$ being 1 if i^{th} task in k^{th} solution is done in mode m . The main purpose of Eq. (19) is to identify the modes to explore via dual values. Finally, Eq. (20) ensures the number of candidates selected from Ω' does not exceed the number of available agents. We apply a linear relaxation to the integer program defined in Eq. (17)-(21) by relaxing the constraint in Eq. (21) and allowing $\theta^k \in [0, 1]$. This relaxation enables faster computation, as algorithms like the simplex method [29] can efficiently solve large-scale linear programs in polynomial time. This is especially useful with a large number of columns in Ω' .

2) *Clustering-based Sub-problem*: In CG, the sub-problem is solved iteratively to populate Ω' . Solving the sub-problem efficiently with high-quality candidate solutions enhances the CG's exploration of the solution space and accelerates convergence to better solutions. However, as the number of tasks and agents increases, the expanded solution space slows down the search for promising candidates. To address this, we introduce a clustering method inspired by cluster-first, route-second heuristics commonly used in routing and scheduling [30]. Our sub-problem solves the MIP problem in Eq. (22) for a single agent at a time, on a restricted set of tasks \mathcal{T}' . All tasks in \mathcal{T} are clustered based on time windows. We use a K-Means clustering [31] approach to create n_c clusters, with n_c being a user-defined parameter. Then \mathcal{T}' is generated by uniformly sampling each cluster. These modifications allow CCG to converge to higher-quality solutions faster than the baseline, as demonstrated in Section IV.

The sub-problem creates a solution for a single agent setup with a restricted task pool \mathcal{T}' . The formulation for the sub-problem is:

$$\begin{aligned} \max_{x_{i \rightarrow j}, y_{i,m}} \sum_{r=0}^R \sum_{i \in \mathcal{T}'} \sum_{j \in \mathcal{T}'} \sum_{m \in \mathcal{M}_i} \lambda_r \cdot f_r(x_{i \rightarrow j}, y_{i,m}, s_i) - \\ \sum_{i \in \mathcal{T}' / \{0\}} (\gamma_i \cdot \sum_{j \in \mathcal{T}'} x_{i \rightarrow j}) - \sum_{i \in \mathcal{T}' / \{0\}} \sum_{m \in \mathcal{M}_i} (\beta_i \cdot y_{i,m}), \end{aligned} \quad (22)$$

Algorithm 1 The clustering-based column generation algorithm

```
1: Input: Problem data  $(\mathcal{A}, \mathcal{T}, \mathcal{M}, T_H, Q$  and associated data  
   for nodes), user preference  $\lambda$ , and algorithm parameters  
    $(n_c, |\mathcal{T}'|, \text{max-iterations, time-limit})$ .  
2: Output: Selected solution for each agent from  $\Omega'$   
3:  $\mathcal{T}_c^{init} \leftarrow$  Divide tasks in  $\mathcal{T}$  to  $n_c$  clusters based on time-windows using  
   K-Means clustering.  
4:  $\Omega' \leftarrow$  Initialize the candidate pool  
5: while True do  
6:    $\theta^k, \gamma_i, \beta_{i,m} \leftarrow$  Solve Eq. (17)-(20) subject to  $\theta^k \in [0, 1]$   
7:    $\mathcal{T}_v \leftarrow$  Initialize empty list to store visited customers.  
8:   for  $i = 1$  to  $|\mathcal{A}|$  do  
9:     if  $i = 1$  then  
10:       $\mathcal{T}_c \leftarrow \mathcal{T}_c^{init}$   
11:     else  
12:       $\mathcal{T}_c \leftarrow$  Create  $n_c$  clusters of remaining tasks  $(\mathcal{T}/\mathcal{T}_v)$  using K-  
        Means clustering.  
13:     end if  
14:      $\mathcal{T}' \leftarrow$  Uniformly sample tasks from  $\mathcal{T}_c$   
15:      $\mathcal{S} \leftarrow$  Solve the sub-problem using Eq. (22)  
16:     if  $\mathcal{S}$  is not empty then  
17:        $\Omega' \leftarrow$  Update solution pool with all feasible solutions from  $\mathcal{S}$   
18:       Update  $\mathcal{T}_v$  with tasks addressed in the best solution of  $\mathcal{S}$   
19:     end if  
20:   end for  
21:   if time-limit reached or max-iterations completed then  
22:     Terminate  
23:   end if  
24: end while  
25: if Terminate then  
26:   Solve Eq (17)-(20) subject to  $\theta^k = \{0, 1\}$   
27: end if  
28: return Selected solution for each agent from  $\Omega'$ 
```

subject to constraints Eq. (3)-(16) and the number of agents is restricted to one. The objective function of the sub-problem, Eq. (22), is a modified variant of Eq. (2), tailored for a single-agent setup and augmented with dual variables from the restricted master problem. Here, γ_i and $\beta_{i,m}$ are non-negative dual of the restricted master problem corresponding to constraints Eq. (18) and Eq. (19) respectively. These dual variables are used to identify promising new candidate solutions. It should be noted that sub-problem The solution of the sub-problem is added to Ω' .

3) *Complete Algorithm:* The CCG algorithm is detailed in Alg. 1. In line 1, the algorithm receives problem parameters, user preferences, and key algorithm settings, including the number of clusters (n_c), the size of the restricted task set ($|\mathcal{T}'|$), maximum iterations, and the time limit. In line 2, initial task clusters \mathcal{T}_c^{init} are formed by dividing \mathcal{T} into n_c clusters based on time windows using K-Means. In line 3, the candidate solution pool Ω' is initialized, with initial solutions generated by randomly selecting tasks and modes while ensuring constraints in Eq. (3)-(16) are satisfied.

From line 5, the restricted master problem and sub-problem are solved iteratively to generate new solutions. The restricted master problem is updated in each iteration based on Ω' (line 6), and the sub-problem's objective is guided by the duals obtained from the restricted master. A list \mathcal{T}_v is initialized to track visited tasks (line 7). The sub-problem is solved iteratively for each agent in \mathcal{A} (lines 8-20).

In the first iteration, task clusters \mathcal{T}_c are initialized to \mathcal{T}_c^{init} (line 10). For subsequent iterations, clusters are recreated from the remaining tasks (line 12). The restricted task set \mathcal{T}' is

formed by uniformly sampling clusters from \mathcal{T}_c (line 14), after which the sub-problem is solved (line 15). Feasible solutions with positive reduced costs are added to Ω' (line 17), and \mathcal{T}_v is updated with tasks corresponding to the best solutions in \mathcal{S} (line 18). This process continues until the stopping criteria—maximum iterations, time limit, or lack of solutions with positive reduced costs—are met (lines ??-23). Upon termination, the restricted master problem is solved to optimality with integrality constraints to obtain the final solution (lines 25-28). A time limit is applied to both the restricted master and sub-problems to maintain time efficiency throughout the process.

C. M³RS for Multi-Robot Disinfection

We consider a fleet of surface disinfection robots deployed in hospital-like environments to provide around-the-clock disinfection. Specifically, we use G-robots [32], which are far-UV-based mobile manipulators designed for surface disinfection. A disinfection mission is a collection of disinfection tasks spread in an environment such as a hospital. Each mission has a specified time horizon within which it should be completed. Further, the tasks must be done in their specified time window. The tasks can have different disinfection dose requirements. This dosage dictates disinfection quality, energy consumption, and the task service time. Each task can be disinfected in a particular set of modes, where the modes have different disinfection dosage options for that task.

The disinfection dosage for UV-based surface disinfection is product of UV exposure duration and irradiance of the UV light source [1]. A higher disinfection dosage would require a longer exposure duration. Typically, the disinfection dosage is expressed in terms of percentage of population reduction. For example, a dosage of D_{90} implies 90% reduction of pathogenic population. A higher reduction percentage requires stronger disinfection dose which in turn leads to longer exposure times. Longer exposure times further implies higher energy consumption. We consider four disinfection modes that are $D_{99.9999}$, $D_{99.99}$, D_{99} , and D_{90} . Here, $D_{99.9999}$ is the strongest disinfection dose with the highest disinfection time and energy consumption as compared to D_{90} [1]. The set of modes can be determined by the acceptable disinfection levels for a surface. So, each task has an associated set of acceptable disinfect doses or modes. The assignment of robots to different tasks and the corresponding modes will be determined by solving M³RS.

For disinfection applications, we have two objectives: i) the number of tasks completed and ii) overall disinfection quality. Higher disinfection quality requires more time and resources, limiting availability for other tasks. For example, critical locations like ICUs in hospitals require higher dosages, so higher quality is preferable. In contrast, areas like waiting rooms or offices do not need the highest quality, and covering the maximum number of surfaces might be preferable. Our formulation creates schedules by using user-specified trade-off requirements. The formulation of M³RS for disinfection application is:

$$\max_{x_i^k \rightarrow j, y_{i,m}^k} \frac{1}{|\mathcal{T}|} \cdot \sum_{k \in \mathcal{A}} \sum_{i \in \mathcal{T}} \sum_{j \in \mathcal{T}} \sum_{m \in \mathcal{M}_i} (\lambda) \cdot x_{i \rightarrow j}^k + (1 - \lambda) \cdot \frac{p_{i,m}}{p^{max}} \cdot y_{i,m}^k, \quad (23)$$

subject to constraints in Eq. (3)-(16). Here, $p_{i,m}$ indicates the quality of disinfection when completing task i in mode m , p^{max} is the highest possible quality of disinfection, and λ represents the user-specified preference. When $\lambda = 1$, the objective ignores quality and focuses on maximizing the number of tasks completed, whereas when $\lambda = 0$, the objective exclusively prioritizes maximizing the quality of disinfection. This mixed integer optimization model can be solved using a standard branch and cut algorithm. However, for larger problem instances, the branch and cut solution has an exploding computation time. The CCG algorithm described in Alg. 1 can be used to effectively compute solutions in such cases.

IV. EVALUATION

In this section, we evaluate the the M^3RS problem and proposed solution strategy of CCG. First, the metrics used for evaluation are defined. Second, the impact of using task-level quality as a decision variable is studied by comparing M^3RS with the classic routing and scheduling in fixed (RS-F) disinfection mode on synthetically generated data. Then, the proposed CCG scheme is compared with a mixed integer programming (MIP) solver. Finally, hardware and simulated case studies are presented.

In each evaluation, multiple problem instances are generated. Each problem instance is characterized by mission time which is given by:

$$T_H = \frac{t_{avg} \times \# \text{ Tasks}}{\eta \times \text{Fleet size}} \quad (24)$$

Here, η is the load factor that is used to simulate missions with different T_H . A higher η leads to tighter mission times. The average task completion time is given by t_{avg} . In our experiments, t_{avg} is considered to be 4.5 minutes. We assume that the robot travels at a fixed speed of 0.5 m/s. We use the MIP solver from IBM's CPLEX [33]. All the evaluations are carried out on machine equipped with an Intel i9 processor with 32 GB RAM.

A. Evaluation Metrics

We define some evaluation metrics to compare the performance of M^3RS and RS-F (Sec. IV-B). The metrics are:

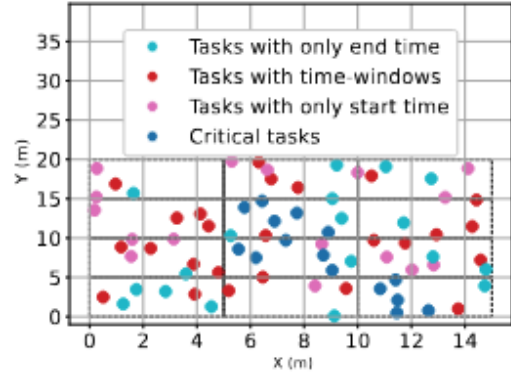
$$SR = \frac{\sum_{k \in \mathcal{A}} \sum_{i \in \mathcal{T}} \sum_{j \in \mathcal{T}} x_{i \rightarrow j}^k}{|\mathcal{T}|} \quad (25)$$

$$DQ = \frac{\sum_{k \in \mathcal{A}} \sum_{i \in \mathcal{T}} \sum_{m \in \mathcal{M}_i} p_{i,m} \cdot y_{i,m}^k}{|\mathcal{T}| \cdot p^{max}} \quad (26)$$

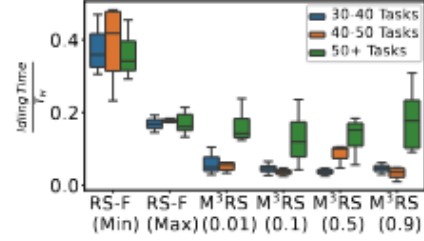
$$MSI = \frac{SR + DQ}{2} \quad (27)$$

$$ATQ = \frac{DQ}{SR} \quad (28)$$

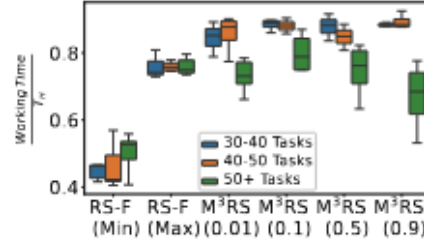
$$QBR = \frac{DQ - DQ^*}{(\bar{Q}_{exp} - \bar{Q}_{exp}^*) + (\bar{M}_{exp} - \bar{M}_{exp}^*)} \quad (29)$$



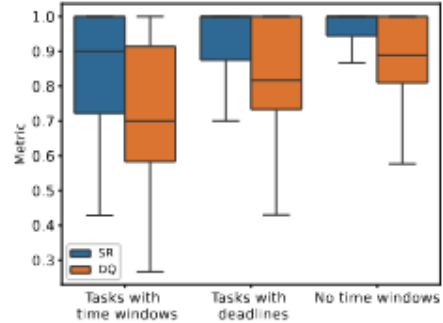
(a) A sample layout for synthetic experiment.



(b) Comparison of idling time to T_H ratio for M^3RS and RS-F for different number of tasks and a fleet size of 4.



(c) Comparison of working time to T_H ratio for M^3RS and RS-F for different number of tasks and a fleet size of 4.



(d) Impact on SR and DQ for different types of time windows. The tasks with time-windows could be critical or non-critical.

Figure 2. (a) A sample layout of a disinfection mission with different task types. (b) & (c) The solution of M^3RS make effective use of agents as indicated by lower idling times and higher working times. (d) It can be seen that tasks available during the entire mission have a higher completion rate (SR) and disinfection quality as well.

The success rate (SR) measures the number of tasks completed successfully (Eq. (25)). The dosage quality (DQ) reflects the disinfection quality of completed tasks (Eq. (26)). The mean success index (MSI) is the average of SR and DQ (Eq. (27)). This metric scores a solution on combined performance on the number of tasks completed and disinfection

quality. The average task quality (ATQ) measures the average disinfection quality received by a serviced task (Eq. (28)).

The quality benefit ratio (QBR) compares a target solution with a baseline solution in terms of the gains made in disinfection quality relative to the resource usage (Eq. (29)). It is a ratio of the difference in disinfection quality to the difference in resource expenditure, measured against a baseline solution. For the target solution, \bar{Q}_{exp} and \bar{M}_{exp} represent the fleet's average energy expenditure and makespan. The RS-F solution serves as the baseline with DQ^* as disinfection quality, \bar{Q}_{exp}^* as average energy, and \bar{M}_{exp}^* as makespan.

In Sec IV-C, we use relative optimal gap (OG) and the objective values (Eq. (23)) are also as a metric. The OG measures the difference between the best known bound on the objective value (o^*) and the current solution's objective value o , is also reported. MIP solvers typically provide this bound by solving a relaxed version of the problem and is given by:

$$OG = \frac{o^* - o}{o^*} \quad (30)$$

B. M^3RS vs RS-F

1) *Baselines*: We assess the impact of the M^3RS formulation, which incorporates quality levels as a decision variable through modes, compared to RS-F which is routing and scheduling with fixed execution modes. The RS-F formulation follows the vehicle routing problem with time windows [34], and we consider two variants: i) RS-F (Min), which uses the mode with the lowest disinfection quality, and ii) RS-F (Max), which uses the mode with the highest quality. For M^3RS we use different values of user preference *i.e.* λ . A higher λ prioritizes quantity over quality. Synthetically generated data is used to benchmark the problems, as detailed in the following paragraph. Both M^3RS and RS-F (Min and Max) are solved using an MIP solver with a 10-minute time limit per problem instance. The evaluation metrics include SR , DQ , MSI , ATQ , and QBR , see Eq (25)-(29). RS-F (Min) is used as the baseline for QBR calculation since it operates in the lowest disinfection mode, allowing us to measure the improvement in disinfection quality relative to resource expenditure. We analyze the solutions based on working and idle time and also discuss the impact of relaxing task time windows for M^3RS .

2) *Synthetic Data Generation*: The synthetic data simulates realistic hospital missions with rectangular layouts of varying sizes. For each layout type, 5 instances are generated and solved. A sample layout is shown in Fig. 2 (a). Four disinfection modes *i.e.* $D_{99.9999}$, $D_{99.99}$, D_{99} , and D_{90} are considered. Each task is randomly assigned one to four disinfection modes, with specific dosage, time, and energy consumption based on [32]. Each problem instance involves a fleet of four robots. We set the value of load factor $\eta = 1$ for this experiment. This ensures that for the disinfection mission there is sufficient time to address the tasks. The mission time (T_H) is calculated using Eq. (24). Tasks are categorized as critical or non-critical. Critical tasks, representing 15-25% of total tasks, must be completed within a specified time window using the highest disinfection dosage of $D_{99.9999}$. These are crucial surfaces, such as those in patient rooms and ICUs. The inequality in

Eq. (3) is replaced by an equality constraint for critical tasks. Non-critical tasks, like those in waiting areas, washrooms, and office spaces, can be skipped but contribute to overall hygiene if addressed. These tasks may have fixed time windows, and deadlines, or be available throughout the mission. All time windows are uniformly sampled from the mission time horizon. A summary of the experimental setup is provided in Table II.

Table II
EXPERIMENT PARAMETERS FOR TESTING IMPACT OF QUALITY.

Quantity	Value
Layout area	150, 200, 225 m^2
Number of tasks	30 – 60
Proportion of Critical tasks	15 – 25%
Avg. task completion time	4.5 mins
Task surface area range	0.5 – 2.2 m^2
η	1
Fleet size	4
Q	6Ah (Amp. hours)

Table III
COMPARISON OF PERFORMANCE METRICS FOR SYNTHETIC PROBLEM INSTANCES. THE COLORS INDICATE THE FIRST, SECOND, AND THIRD RANKING FOR A GIVEN METRIC. THE SOLUTIONS OF M^3RS PERFORM WELL ON BOTH QUALITY AND QUANTITY OBJECTIVES AS INDICATED BY DIFFERENT METRICS. THE NUMBER OF TASKS RANGE FROM 30 – 60 AND THE ROBOT FLEET SIZE IS FOUR.

Metric	RS-F (Min)	RS-F (Max)	M^3RS -0.01	M^3RS -0.1	M^3RS -0.5	M^3RS -0.9
SR	1.0 ± 0.0	0.847 ± 0.082	0.906 ± 0.078	0.912 ± 0.072	0.941 ± 0.068	0.973 ± 0.042
DQ	0.452 ± 0.031	0.757 ± 0.083	0.820 ± 0.078	0.829 ± 0.097	0.789 ± 0.095	0.750 ± 0.124
MSI	0.726 ± 0.016	0.802 ± 0.082	0.863 ± 0.072	0.870 ± 0.079	0.865 ± 0.073	0.862 ± 0.08
ATQ	0.452 ± 0.031	0.894 ± 0.024	0.906 ± 0.063	0.909 ± 0.070	0.839 ± 0.082	0.768 ± 0.104
QBR	N/A	0.331 ± 0.064	0.364 ± 0.082	0.391 ± 0.117	0.331 ± 0.104	0.297 ± 0.129

3) *Results*: The mean and standard deviation of the performance metrics for solutions of RS-F and M^3RS variants are presented in Table III. RS-F (Min) achieves the highest success rate (SR), addressing all tasks. This is because the lowest disinfection dosage is used by default, reducing disinfection time and increasing SR , but at the cost of lower disinfection quality (DQ). Conversely, RS-F (Max) provides higher DQ but lower SR . The higher disinfection quality requires more time, limiting agents' ability to complete other tasks. The solutions of M^3RS outperform the RS-F baselines in the combined metric (MSI), offering a better balance between SR and DQ . The solutions of M^3RS admit better DQ and ATQ scores. The QBR scores show that solutions of M^3RS offer better quality improvement relative to the additional resource expenditure (energy and time). This suggests that considering disinfection quality through variable disinfection modes improves overall disinfection quality while maintaining or improving task completion rates.

We further analyze the missions by looking at the ratio of idle time to task servicing time, as well as the SR and DQ for different time-window types (see Fig. 2 (a)-(c)). The solution of M^3RS show less idle time and more working time, indicating better use of mission time, see Fig. 2 (a)-(b). Using variable disinfection modes likely saves time and energy, which can be spent on disinfecting more tasks or improving quality for others, depending on the user preference

Table IV

COMPARISON OF OG VALUES BETWEEN MIP SOLVER AND CG SOLUTIONS. COLORS REPRESENT THE FIRST, SECOND, AND THIRD RANKINGS FOR THE OG METRIC. CCG SOLUTIONS ACHIEVE BETTER OG VALUES AS COMPARED TO THE MIP SOLVER FOR THE SAME COMPUTATION TIME LIMIT.

Method	Number of Tasks and Robots, $\eta = 1.0, \lambda = 0.9$				Number of Tasks and Robots, $\eta = 2.0, \lambda = 0.9$			
	120-4	150-5	175-5	200-6	120-4	150-5	175-5	200-6
MIP	0.131 ± 0.034	0.278 ± 0.113	0.247 ± 0.046	0.353 ± 0.024	0.253 ± 0.032	0.290 ± 0.061	0.570 ± 0.065	0.488 ± 0.039
CCG ($K = 2$)	0.136 ± 0.050	0.110 ± 0.024	0.218 ± 0.024	0.300 ± 0.018	0.116 ± 0.015	0.177 ± 0.039	0.455 ± 0.011	0.380 ± 0.006
CCG ($K = 4$)	0.126 ± 0.009	0.121 ± 0.034	0.211 ± 0.017	0.302 ± 0.023	0.097 ± 0.045	0.179 ± 0.021	0.434 ± 0.013	0.363 ± 0.014
CCG ($K = 6$)	0.110 ± 0.025	0.132 ± 0.025	0.208 ± 0.010	0.305 ± 0.021	0.107 ± 0.025	0.180 ± 0.021	0.453 ± 0.026	0.358 ± 0.029
CCG ($K = 8$)	0.133 ± 0.031	0.102 ± 0.022	0.220 ± 0.019	0.308 ± 0.009	0.106 ± 0.047	0.184 ± 0.020	0.446 ± 0.019	0.355 ± 0.025
Method	Number of Tasks and Robots, $\eta = 1.0, \lambda = 0.1$				Number of Tasks and Robots, $\eta = 2.0, \lambda = 0.1$			
	120-4	150-5	175-5	200-6	120-4	150-5	175-5	200-6
MIP	0.124 ± 0.032	0.181 ± 0.021	0.153 ± 0.014	0.215 ± 0.019	0.409 ± 0.031	0.586 ± 0.013	0.5200 ± 0.026	0.602 ± 0.021
CCG ($K = 2$)	0.103 ± 0.018	0.144 ± 0.037	0.188 ± 0.022	0.205 ± 0.016	0.357 ± 0.037	0.483 ± 0.015	0.425 ± 0.018	0.514 ± 0.021
CCG ($K = 4$)	0.116 ± 0.018	0.126 ± 0.019	0.156 ± 0.029	0.197 ± 0.020	0.310 ± 0.023	0.491 ± 0.016	0.436 ± 0.021	0.517 ± 0.018
CCG ($K = 6$)	0.132 ± 0.027	0.150 ± 0.034	0.162 ± 0.032	0.201 ± 0.020	0.349 ± 0.031	0.483 ± 0.012	0.418 ± 0.009	0.520 ± 0.014
CCG ($K = 8$)	0.116 ± 0.019	0.134 ± 0.015	0.198 ± 0.010	0.181 ± 0.027	0.336 ± 0.011	0.491 ± 0.012	0.424 ± 0.015	0.502 ± 0.025

i.e. λ . RS-F (Max) shows higher idle time and lower working time than M³RS, as disinfection in the highest modes requires robots to arrive at or before a task's time window. Early arrivals lead to waiting, limiting task completion and resulting in lower SR and DQ compared to M³RS.

When examining SR and DQ across time-window types, tasks available throughout the mission have the best performance, while those with limited time windows perform worse, see Fig. 2 (c). This suggests that relaxing time constraints where possible could lead to better overall performance.

C. Performance of CCG

1) *Baselines*: The performance of solving M³RS with CCG is compared with that of directly solving using MIP solver. For CCG, we report results with varying number of clusters i.e. $K \in [2, 4, 6, 8]$. The performance is evaluated in terms of the relative optimality gap (OG) given by Eq (30). For CCG, we use the best bound from the MIP solver to compute the OG .

2) *Setup*: For this, four problem types are considered with a number of tasks and robots mentioned in Table. IV. For each problem type, 5 instances are generated using the procedure outlined in Sec. IV-B. User preference for each instance is sampled from $\lambda \in [0.1, 0.9]$, with higher λ values prioritizing task completion over disinfection quality. We use load factors $\eta = 1$ and $\eta = 2$, where higher η simulates missions with shorter T_H , providing less time for mission completion. The mission time (T_H) is calculated using Eq (24). The time limit for MIP solver and CCG is set to 10 minutes. We further report the performance with time limit for MIP set to 25 minutes.

3) *Discussion*: The mean and standard deviation of the OG metric for MIP and CCG with time limit set to ten minutes is reported in Table IV. The change in OG for MIP solver relative to CCG, with time limit for MIP solver set to 25 minutes is reported in Table V. The OG achieved by CCG solutions is consistently better than that of MIP solver with the same time limit, see Table IV. Further, it is seen with increased time limit the performance of CCG remains comparable or better than MIP solver while being 2.5 \times faster. This indicates that clustering and sampling approach coupled with column generation provides an effective way to find good

solution in shorter time as compared to MIP solver. Generally, clustering improves OG values, with more clusters benefiting larger instances.

Table V

DIFFERENCE OF AVERAGE OPTIMALITY GAP (OG) BETWEEN CCG AND THE MIP SOLVER ACROSS VARIOUS INSTANCES. A 25-MINUTE TIME LIMIT IS SET FOR THE MIP SOLVER. POSITIVE DIFFERENCES INDICATE BETTER OG FOR THE MIP SOLVER, WHILE NEGATIVE VALUES FAVOR CCG. COLORS REPRESENT MIP OUTPERFORMING CCG AND CCG OUTPERFORMING MIP. CCG ACHIEVES COMPARABLE OR BETTER OG WHILE BEING APPROXIMATELY 2.5 \times FASTER THAN THE MIP BASELINE.

Metric	η	λ	120-4	150-5	175-5	200-6
$OG_{CCG} - OG_{MIP}$	1.0	0.9	0.038	-0.084	-0.058	-0.077
		0.1	0.022	-0.052	-0.007	-0.026
	2.0	0.9	0.003	-0.154	-0.074	-0.150
		0.1	-0.029	-0.080	-0.091	-0.105

D. Simulated and Hardware Case Study

1) *Simulation and Hardware Experiment Setup*: Multiple disinfection mission instances are generated for a simulated environment. Each disinfection mission is characterized by mission time, time windows for each task, and number of robots used in the mission. The simulated environment consists of 20 tables as disinfection surfaces spread across two rooms. The fleet size considered in the range, $|\mathcal{A}| = 2 - 5$. The mission time is calculated using Eq. 24. The entire simulated experiment is conducted in ROS [35] and Gazebo environment [36]. A simulated mission is depicted in Fig 3 (b).

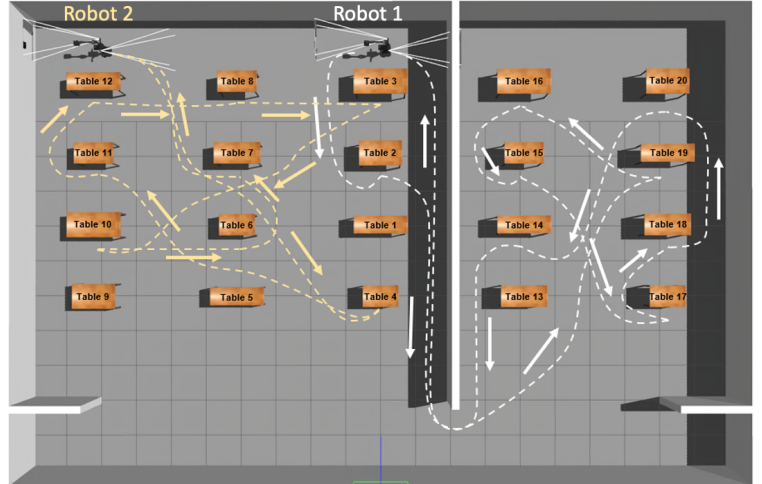
For the hardware case study, we use two G-robots (shown in Fig. 3 (a)) for a disinfection mission consisting of six tables. Each table can be disinfected in three disinfection modes, i.e. $D_{99.99}$, D_{99} , and D_{90} . The entire disinfection mission must be completed in 17 minutes.

For both experiments, M³RS is solved for two preferences: $\lambda = 0.9$ and 0.1 for each mission. The optimization model is solved in CPLEX [33]. The metrics reported include SR , DQ , MSI , and average lateness of the robot in task completion.

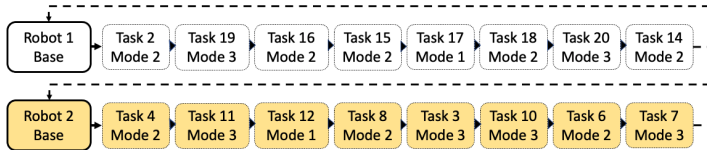
2) *Discussion*: The metrics for simulated and hardware case studies are reported in Table VI. The example of generated route sequences in simulated experiment is visualized



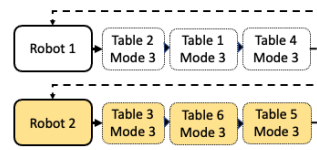
(a) A team of G-robots disinfecting tables.



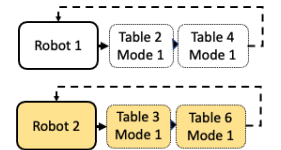
(b) The simulated environment with 20 tasks and 2 robots.



(c) The route sequences for simulated mission with 20 tasks, 2 robots, T_H of 0.4 hours and $\lambda = 0.9$.



(d) The route sequence for hardware experiment with $\lambda = 0.9$.



(e) The route sequence for hardware experiment with $\lambda = 0.1$.

Figure 3. (a) A team of G-robots [32] disinfecting tables. (b) The routes of two robots executing various tasks in the simulated environment. The route of the first robot is highlighted in white and for the second robot yellow is used. (c) The route sequence taken by each robot in the simulated mission. For $\lambda = 0.9$, maximization of the number of tasks completed has more emphasis than the quality of disinfection. As a result, most of the tasks are done in higher modes. (d) & (e) The route sequence taken by each robot for the hardware mission with $\lambda = 0.9$ and 0.1 . For $\lambda = 0.9$, the emphasis is on disinfecting all the tables at higher disinfection modes. Whereas, for $\lambda = 0.1$, the emphasis is on ensuring high-quality disinfection rather than disinfecting all tables.

in Fig. 3 (b)-(c). The route sequence for hardware experiments is shown in Fig. 3 (d)-(e). From Table VI, it can be seen that a decent SR is achieved in all missions. Even for missions with tight T_H the SR is high. Therefore, a larger robotic fleet would be necessary to compensate for tighter mission times in order to service as many tasks as possible. For missions with shorter T_H , there is a decline in DQ metric. This is because with tighter mission times, each task has a smaller time window, which means many of the tasks cannot be performed in higher disinfection modes. A possible remedy could be to enable robots to collaborate on different tasks. Finally, there are some minor delays observed in terms of task completion times for simulation and hardware implementation. These delays are caused by slightly longer path navigation times. Such delays can be accounted for by introducing chance constraints to model stochasticity in the system.

V. CONCLUSIONS AND FUTURE WORK

In this work, we proposed M^3RS , a novel multi-objective formulation that routes and schedules a team of agents to accomplish various tasks in a mission. The agents can perform the task in one of many available modes. Each mode has distinct task quality, resource consumption, and service times. We first propose a mixed-integer linear programming model for M^3RS . Then, a column generation approach is presented to tackle larger instances with a faster computation time. We showcase the utility of M^3RS in multi-robot disinfection

Table VI
RESULTS FOR SIMULATED AND HARDWARE EXPERIMENTS.

Num. of tasks and robots	T_H (hrs)	λ	SR	DQ	MSI	Avg. Lateness (s)
20-2	0.40	0.9	0.80	0.57	0.63	1.9
		0.1	0.70	0.71	0.60	6.2
20-3	0.21	0.9	0.80	0.51	0.60	30.1
		0.1	0.75	0.56	0.58	1.4
20-4	0.20	0.9	0.95	0.55	0.74	33.6
		0.1	0.90	0.60	0.72	19.1
20-5	0.16	0.9	0.80	0.57	0.68	29.4
		0.1	0.75	0.62	0.68	33.7
6-2*	0.28	0.9	1.00	0.40	0.70	27.0
		0.1	0.67	1.00	0.65	32.0

* = Results for hardware experiments.

applications. The experiments suggest that our solution for M^3RS provides more flexibility to users to select solutions based on desired preferences. The current approach is limited as it assumes a deterministic environment, unlike real-world scenarios. Generating the entire Pareto front is computationally expensive, particularly for larger instances. Our future work will extend M^3RS to incorporate elements like stochastic travel times, dynamic arrival of tasks and realistic issues like robot breakdown. Further, we aim to tightly integrate the robot path planning with the decision making framework provided by M^3RS . Finally, we will investigate using deep reinforcement learning techniques to generate good quality solutions in real-time.

ACKNOWLEDGEMENTS

We would like to thank Mr. Matthew Lisondra for all the support with the experiments.

REFERENCES

- [1] I. Mehta, H.-Y. Hsueh, S. Taghipour, W. Li, and S. Saeedi, "Uv disinfection robots: a review," *RAS*, vol. 161, p. 104332, 2023.
- [2] G. A. Korsah, A. Stentz, and M. B. Dias, "A comprehensive taxonomy for multi-robot task allocation," *IJRR*, vol. 32, no. 12, pp. 1495–1512, 2013.
- [3] B. P. Gerkey and M. J. Matarić, "A formal analysis and taxonomy of task allocation in multi-robot systems," *IJRR*, vol. 23, no. 9, pp. 939–954, 2004.
- [4] S. Hayat, E. Yanmaz, C. Bettstetter, and T. X. Brown, "Multi-objective drone path planning for search and rescue with quality-of-service requirements," *Autonomous Robots*, vol. 44, no. 7, pp. 1183–1198, 2020.
- [5] E. F. Flushing, L. M. Gambardella, and G. A. Di Caro, "Simultaneous task allocation, data routing, and transmission scheduling in mobile multi-robot teams," in *2017 IROS*. IEEE, 2017, pp. 1861–1868.
- [6] A. Botros, B. Gilhuly, N. Wilde, A. Sadeghi, J. Alonso-Mora, and S. L. Smith, "Optimizing task waiting times in dynamic vehicle routing," *IEEE Robotics and Automation Letters*, 2023.
- [7] J. Miller and J. P. How, "Predictive positioning and quality of service ridesharing for campus mobility on demand systems," in *2017 IEEE International Conference on Robotics and Automation (ICRA)*. IEEE, 2017, pp. 1402–1408.
- [8] M. Calzavara, M. Faccio, and I. Granata, "Multi-objective task allocation for collaborative robot systems with an industry 5.0 human-centered perspective," *The IJAMT*, vol. 128, no. 1-2, pp. 297–314, 2023.
- [9] K. Braekers, K. Ramaekers, and I. Van Nieuwenhuysse, "The vehicle routing problem: State of the art classification and review," *Computers & industrial engineering*, vol. 99, pp. 300–313, 2016.
- [10] A. Bogyrbayeva, M. Meraliyev, T. Mustakhov, and B. Dautbayev, "Learning to solve vehicle routing problems: A survey," *arXiv preprint arXiv:2205.02453*, 2022.
- [11] A. Expósito, J. Brito, J. A. Moreno, and C. Expósito-Izquierdo, "Quality of service objectives for vehicle routing problem with time windows," *Applied Soft Computing*, vol. 84, p. 105707, 2019.
- [12] G. Kordi, A. Divsalar, and S. Emami, "Multi-objective home health care routing: a variable neighborhood search method," *Optimization Letters*, vol. 17, no. 9, pp. 2257–2298, 2023.
- [13] M. Di Mascolo, C. Martinez, and M.-L. Espinouse, "Routing and scheduling in home health care: A literature survey and bibliometric analysis," *Computers & Industrial Engineering*, vol. 158, p. 107255, 2021.
- [14] O. M. Anli, M. C. Caramanis, and I. C. Paschalidis, "Tractable supply chain production planning, modeling nonlinear lead time and quality of service constraints," *Journal of Manufacturing Systems*, vol. 26, no. 2, pp. 116–134, 2007.
- [15] M. Lahijanian, M. Svorenova, A. A. Morye, B. Yeomans, D. Rao, I. Posner, P. Newman, H. Kress-Gazit, and M. Kwiatkowska, "Resource-performance tradeoff analysis for mobile robots," *IEEE RAL*, vol. 3, no. 3, pp. 1840–1847, 2018.
- [16] Y. Y. Liau and K. Ryu, "Genetic algorithm-based task allocation in multiple modes of human-robot collaboration systems with two cobots," *The IJAMT*, vol. 119, no. 11-12, pp. 7291–7309, 2022.
- [17] C. Ferreira, G. Figueira, and P. Amorim, "Scheduling human-robot teams in collaborative working cells," *IJPE*, vol. 235, p. 108094, 2021.
- [18] S. Hartmann and D. Briskorn, "An updated survey of variants and extensions of the resource-constrained project scheduling problem," *EJOR*, vol. 297, no. 1, pp. 1–14, 2022.
- [19] J. Alcaraz, C. Maroto, and R. Ruiz, "Solving the multi-mode resource-constrained project scheduling problem with genetic algorithms," *JORS*, vol. 54, no. 6, pp. 614–626, 2003.
- [20] M. Caramia and S. Giordani, "A fast metaheuristic for scheduling independent tasks with multiple modes," *Computers & Industrial Engineering*, vol. 58, no. 1, pp. 64–69, 2010.
- [21] C. Tilk, K. Olkis, and S. Irnich, "The last-mile vehicle routing problem with delivery options," *Or Spectrum*, vol. 43, no. 4, pp. 877–904, 2021.
- [22] M. Seyfi, M. Alinaghian, E. Ghorbani, B. Çatay, and M. S. Sabbagh, "Multi-mode hybrid electric vehicle routing problem," *Transportation Research Part E: Logistics and Transportation Review*, vol. 166, p. 102882, 2022.
- [23] L. Zhang, J. Zhao, E. Lamon, Y. Wang, and X. Hong, "Energy efficient multi-robot task allocation constrained by time window and precedence," *IEEE Transactions on Automation Science and Engineering*, 2023.
- [24] I. Kara, G. Laporte, and T. Bektas, "A note on the lifted miller-tucker-zemlin subtour elimination constraints for the capacitated vehicle routing problem," *EJOR*, vol. 158, no. 3, pp. 793–795, 2004.
- [25] S. N. Kumar and R. Panneerselvam, "A survey on the vehicle routing problem and its variants," 2012.
- [26] E. Uchoa, D. Pecin, A. Pessoa, M. Poggi, T. Vidal, and A. Subramanian, "New benchmark instances for the capacitated vehicle routing problem," *European Journal of Operational Research*, vol. 257, no. 3, pp. 845–858, 2017.
- [27] J. Desrosiers and M. E. Lübbecke, "A primer in column generation," in *Column generation*. Springer, 2005, pp. 1–32.
- [28] M. E. Lübbecke and J. Desrosiers, "Selected topics in column generation," *Operations research*, vol. 53, no. 6, pp. 1007–1023, 2005.
- [29] H. Nabli, "An overview on the simplex algorithm," *Applied Mathematics and Computation*, vol. 210, no. 2, pp. 479–489, 2009.
- [30] F. Liu, C. Lu, L. Gui, Q. Zhang, X. Tong, and M. Yuan, "Heuristics for vehicle routing problem: A survey and recent advances," *arXiv preprint arXiv:2303.04147*, 2023.
- [31] C. M. Bishop, "Mixture models and the em algorithm," *Microsoft Research, Cambridge*, 2006.
- [32] I. Mehta, H.-Y. Hsueh, N. Kourtzanidis, M. Brylka, and S. Saeedi, "Far-uvc disinfection with robotic mobile manipulator," in *2022 International Symposium on Medical Robotics (ISMR)*. IEEE, 2022, pp. 1–8.
- [33] P. Laborie, J. Rogerie, P. Shaw, and P. Vilím, "Ibm ilog cp optimizer for scheduling: 20+ years of scheduling with constraints at ibm/ilog," *Constraints*, vol. 23, pp. 210–250, 2018.
- [34] B. Kallehauge, J. Larsen, O. B. Madsen, and M. M. Solomon, *Vehicle routing problem with time windows*. Springer, 2005.
- [35] M. Quigley, K. Conley, B. Gerkey, J. Faust, T. Foote, J. Leibs, R. Wheeler, and A. Y. Ng, "ROS: an open-source Robot Operating System," in *ICRA workshop on open source software*, vol. 3, no. 3.2. Kobe, Japan, 2009, p. 5.
- [36] N. Koenig and J. Hsu, "The many faces of simulation: Use cases for a general purpose simulator," in *Proc. of the ICRA*, vol. 13, 2013, pp. 10–11.